공학석사학위논문

실린더내 직분사 엔진에서의 벽면 충돌 및 액막 모델링

Modeling of Spray-Wall Impingement and Fuel Film for Direct-Injection Spark-Ignition Engines

2017 년 8 월

서울대학교 대학원

기계항공공학부

김 정 현

실린더내 직분사 엔진에서의 벽면 충돌 및 액막 모델링

Modeling of Spray-Wall Impingement and Fuel Film for Direct-Injection Spark-Ignition Engines

지도교수 민 경 덕

이 논문을 공학석사 학위논문으로 제출함

2017 년 7 월

서울대학교 대학원

기계항공공학부

김 정 현

김정현의 공학석사 학위논문을 인준함

2017 년 6 월

위 원 장 _____

부위원장 _____

위 원 _____

Abstract

Modeling of Spray-Wall Impingement and Fuel Film for Direct-Injection Spark-Ignition Engines

Junghyun Kim
Department of Mechanical and Aerospace Engineering
The Graduate School
Seoul National University

Since the amount of emitted CO2 is directly related to car fuel economy, the attention is being drawn to DISI engine which has better fuel economy than conventional gasoline engine. Cooling effect, high volumetric efficiency and high compression ratio are main advantage of the DISI engine. However, the fact that increased inhomogeneity of air-fuel mixture and fuel film on the wall due to spray impingement during cold start make particulate matter(PM) come to the fore. Conducting experiment with large numbers of engine geometries and injection strategies are time consuming methods and expensive to proceed. Thus, reliable simulation model should be developed to reduce the cost for

engine development.

For accurate prediction of PM emission, the behavior of the spray and fuel film after spray-wall impingement needs to be predicted correctly. Thus, accurate spray model and film model are prerequisite. The existing models, however, are found to have relatively large error when compared with the experimental results. The rebound spray height is over-estimated while the area of the fuel film is under-estimated. The reasons for such disagreement between the simulation results and the experimental results are the assumptions used in the previous models. The previous models only considered the low speed collision condition such as diesel engine which has relatively short penetration length due to its injection pressure. Therefore, the dissipation energy can be successfully calculated from weber number and surface tension energy. However, the high-speed collision occurs in DISI engine. The droplet kinetic energy is too large to reduce meaningful amount by weber number and surface energy. Thus, in modified model, the amount of dissipation energy is determined within specific range. As a result, it was possible to reduce the number of model constants. To consider 2-D spray-wall impingement phenomenon more accurately, the number of child parcels derived from the parent parcel is increased from two to four. Increasing the number of child parcels, it is possible to consider the normal and tangential momentum

component.

Finally, the modified model is validated with experiments. The Mie-scattering images of iso-octane spray near wall were acquired at various temperature and injection pressure to measure rebound spray radius and height. Compared to the existing models, the modified model shows the best agreement with the experimental results without case-dependent changes to the model constant.

Keywords: Droplet Wall Impingement, Wall film, Computational Fluid Dynamics, Mie scattering, Direct-Injection Spark-Ignition.

Student Number: 2015-22712

Contents

List of Figures

List of Tables

Nomenclature

A	area
d_l	droplet diameter
e	restitution coefficient
g	gravity constant
h	enthalpy
La	Laplace number
m_I	impinging parcel mass
m_s	sum of total mass child parcels
N_1, N_2, N_3, N_4	the number of droplets in each parcel
Oh	Ohnesorge number
P	pressure
Re	Reynolds number
R	radius of drop on plane
r_m	mass ratio of m_s and m_I

U_I	impinging droplet velocity
u_i, u_j	child parcel velocity
u_d^0	x component of impinging parcel velocity
u_d'	x component of rebounded parcel velocity
V	droplet velocity
v_d^0	y component of impinging parcel velocity
v_d'	y component of rebounded parcel velocity
δ	film thickness
Δt	time difference
θ_c	contact angle
θ_I	incoming angle of attack
μ	droplet viscosity
ρ_d	droplet density
σ	droplet surface tension

Acronym

AVL	Anstalt für Verbrennungskraftmaschinen List
CFD	Computational Fluid Dynamics
CO2	Carbon Dioxide
DISI	Direct-Injection Spark-Ignition
ECU	Engine Control Unit
k-ε RNG	k-ε Re-Normalization Group
LED	Light Emitting Diode
NEDC	New European Driving Cycle
NIST	National Institute of Standards and Technology
PDF	Probability Density Function
PFI	Port Fuel Injection
PM	Particle Matter
TTL	Transistor-Transistor Logic

Chapter 1. Introduction

1.1 Background

The mileage restriction goes harder globally. Europe target 70g/km in 2025, America target 89g/km in 2025, South Korea target 97g/km in 2020. In order to satisfy target restriction, the DISI engine which has cooling effect, high volumetric efficiency and high tumble ratio is good solution [1].

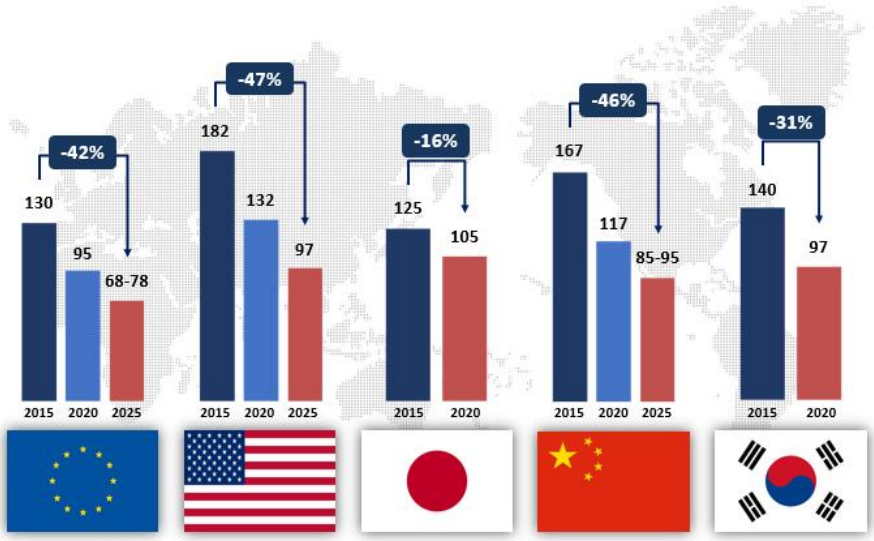

Figure 1. The CO2 regulation of each country [1]

However, the problem that local rich air fuel mixture generate PM come to the fore. The engine researcher study engine PM to satisfy the restriction which goes stronger than before. PM is emitted 70% during cold start [2]. This is because not sufficient time to warm up engine from low temperature (coolant,

cylinder wall, intake air, etc.) increase inhomogeneity of air fuel mixture. Because low wall temperature deters film evaporation, the mixture near the film goes rich. This is one of the main reason which the PM is generated from the rich mixture. Combustion efficiency and emission are strongly affected by the wall impingement and wall film formation phenomenon. They are related closely. Thus, spray shape, wall impingement and film formation should be simultaneously studied.

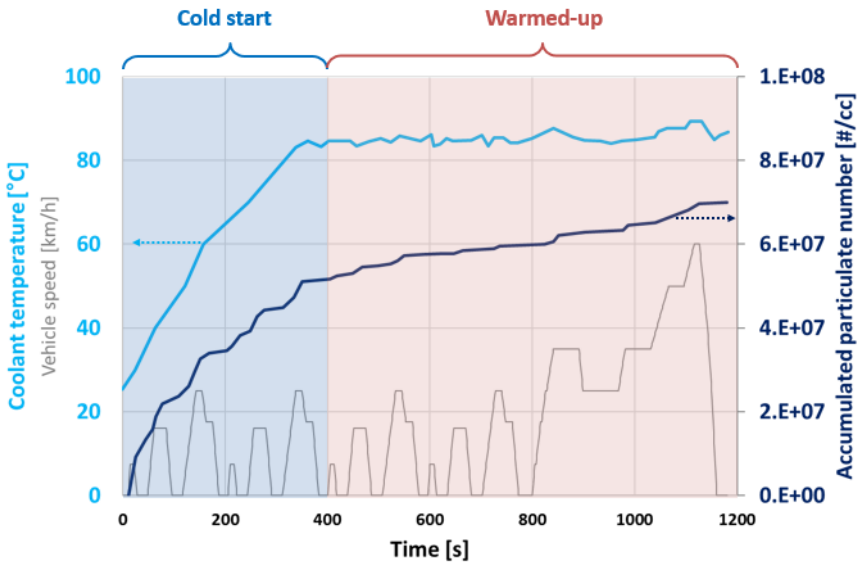

Figure 2. Particulate emission according to driving condition [2]

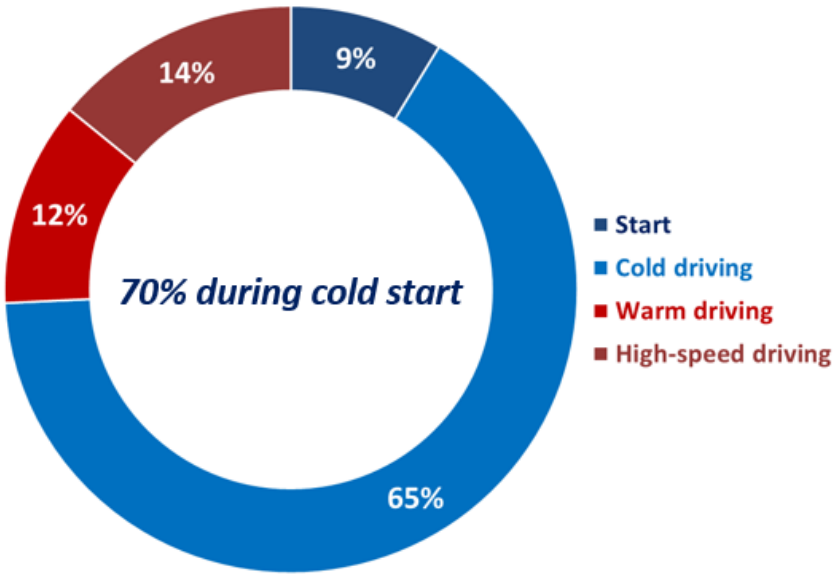

Figure 3. Proportion of the PM emission during NEDC cycle [2]

However, conducting experiment with large numbers of engine geometries and injection strategies are time consuming methods and expensive to proceed. Thus, reliable simulation model should be developed to reduce the cost for engine development.

The pre-existing bai model simulate wall impingement phenomenon by splitting one parent parcel to two child parcels. The model shows good agreement with diesel experiments [3]. The dissipation energy is defined as the starting energy to splash from parent parcel, then it is assumed that the splash phenomena are occurred when parent parcel has above criteria energy. The diameter of child parcel derived by splash phenomena is distributed evenly under diameter of parent parcel. Also, the tangential velocity of child parcels is

determined by model constant. After that, the modified model is introduced. It is assumed that the dissipation energy is in proportional to parent kinematic energy within the specific range, to expend the coverage of the model from diesel in order to gasoline injection which has faster parcel before collision. The film model and transition logic is developed to describe film behavior considering wall impingement. However, assumption of models that the parcels have identical mass and the diameter of parcel is determined to random value generate slight error on diameter distribution and velocity. Moreover, the assumption that two child parcels are generated from a parent parcel consider only radial momentum transfer. Thus, it shows impractical behavior.

Kim develop modified model based on experimental data [4]. The criterial of splash is redefined by considering experimental data from Mundo and the amount of energy dissipation is modified. Also, the model has strength to describe diameter distribution and velocity distribution by considering child parcels behavior based on experimental data. In addition, the impingement phenomenon is simulated by splitting four child parcels to describing 2-D momentum transfer. However, the Kim model has limitation at film modeling. Kim model consider film-air shear force as film momentum source to describe movement of film [5]. Therefore, it is not enough to simulate the film behavior of DISI engine.

In recent study, the boundary of study is expended over leidenfrost temperature using infrared camera [6]. The previous models assumed that there is no film over leidenfrost temperature. However, the experimental results showed that the surface temperature is locally cooled more than 30K. It is

sufficient temperature to generate film by considering the time between spray timing and ignition timing in engine condition. It is solved by calculating surface temperature and adopted to initial condition. The fundamental solution is the heat transfer effect is considered to predict film behavior as simulation progresses.

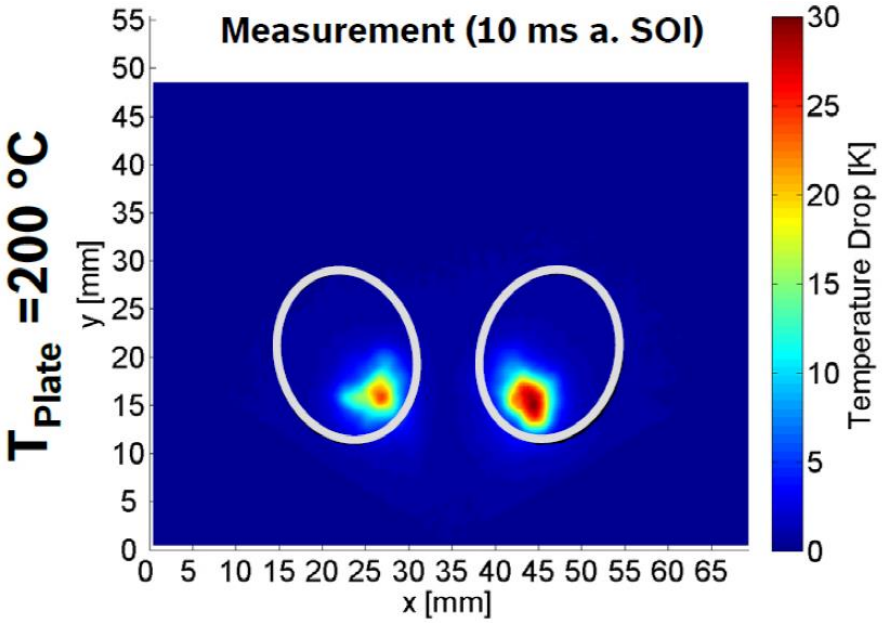

Figure 4. Measured temperature distributions for a 200℃ initial plate temperature

Contact angle is affected by flow rate, temperature, width of rivulet. Considering this fact, a method of determining contact line is being studied [7]. When the film flow on inclined surface, the method to describe fingering effect is studied. Although The simulation is progressed without wall impingement phenomenon, it is useful to predict the boundary film behavior that considering contact angle difference.

Nowadays, the rig experiments are conducted in restricted condition. By experimenting with specific components in a controlled environment, the rig experiment reduces the number of factors affecting the experiment results. In the same manner, the sprays are captured by laser and camera in static chamber to validate spray model. The sprays are measured in various ambient temperature and pressure which represent engine condition. The results of experiments show that modified model can predict rebound spray radius and height precisely.

In this work, the modified wall impingement model and film model are suggested. Then the models had compared each other to show the improvement. Bai wall impingement model has limitation which assume the child parcels mass are equivalent and tangential velocity is determined by a coefficient which can gain from experience. Film formation model predict symmetric momentum transfer, because it assumes 1-D momentum transfer. In this model, wall impingement phenomenon is well simulated with lesser model constant than bai model and 2-D momentum transfer source is described in order to capture non-symmetric momentum transfer phenomenon.

1.2 Previous Research

1.2.1 Bai Model

Droplet wall impingement model and overview of the droplet impingement regimes were suggested by Bai and Gosman [3]. Wall impingement parameters such as droplet velocity, droplet diameter, surface tension, surface roughness, density, viscosity are non-dimensionalized to handle wall impingement phenomenon.

Reynolds number

$$Re = \frac{\rho_d V d_l}{\mu} \tag{1.1}$$

Weber number

$$We = \frac{\rho_d V^2 d_l}{\sigma} = \frac{Droplet\ Kinetic\ Energy}{Surface\ Energy} \tag{1.2}$$

Laplace number

$$La = \frac{\rho_d \sigma d_l}{\mu^2} = \frac{1}{Oh^2} = \frac{Surface\ Tension}{Viscous\ Forces} \tag{1.3}$$

$$K = \sqrt{We\sqrt{Re}} \tag{1.4}$$

Where ρ_d, μ, V and σ are the density, viscosity, droplet normal incident velocity, surface tension of fuel, respectively.

The non-dimensionalized temperature of the wall are given by equation (1.5).

$$\frac{T_d}{T_B}, \frac{T_w}{T_B}, \frac{T_w}{T_{PA}}, \frac{T_w}{T_N}, \frac{T_w}{T_{PR}}, \frac{T_w}{T_{Leid}} \tag{1.5}$$

T_B : Boiling Temperature

T_{PA} : Pure Adhesion Temperature

(Below this temperature, adhesion is occurred with low impact energy parent droplets)

T_N : Nakayama temperature (maximum evaporation)

T_{PR} : Pure Rebound Temperature

(Below this temperature, rebound is occurred with low impact energy parent droplets)

T_{Leid} : Leidenfrost Temperature (minimum evaporation)

The criteria and condition are based on experiments and paper [3]. The criteria and condition are described below:

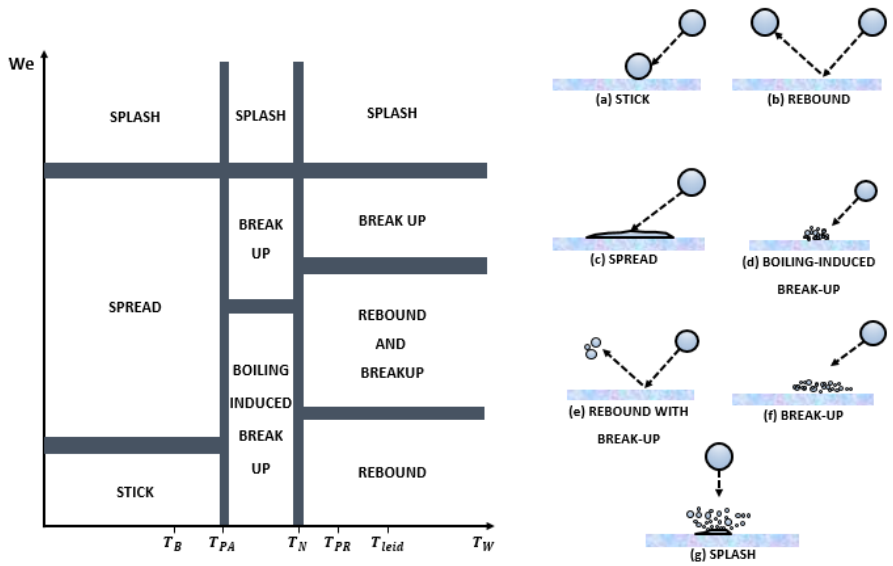

Figure 5. Type of spray-wall impingement phenomenon and its criteria [3]

The described criteria of region are limited. However, researcher can get overall qualitative sight. The bigger weber number, the stronger parent parcel momentum is transfer to the wall. Then each droplet tends to be splashed because it is much larger than surface energy. Also, the higher temperature parcel conserves the better its momentum due to the boiling induced break up effect is increased when high temperature parcel collides. When the temperature of the plate is over leidenfrost temperature, the lower part of the droplet evaporates immediately and generate the vapor layer. Thus, the droplet float above the layer and move along the layer. Because the area between droplet and surface is minimum, the droplet can survive about 10 times longer than before leidenfrost temperature. In this regime, it is assumed that film is not deposited on the surface. Furthermore, the vapor layer absorbs the shocks from

impingement and preserve the parent droplet momentum.

The Bai model assumes that the child parcels split from parent parcel moves along the plane which the parent parcel velocity vector and wall normal vector belongs. Thus, the momentum is transferred only in the direction of the parent parcel velocity due to limitation of assumption. The main proportion of film momentum source is come from parcel impingement which has radial direction. Thus, film spreads symmetrically. There is another problem that the model only covers low-speed collision case because only diesel spray is analyzed. Due to short penetration length of diesel spray, the momentum of the parent parcel relatively low. Thus, the Bai model assume that dissipation energy can be calculated properly with surface tension energy and weber number. In Bai model, the tangential velocity magnitude is defined by model constant. However, not only normal velocity but also tangential velocity should be calculated by equation for precise simulation.

1.2.2 Bai Renewal Model

Bai renewal model was developed to cover gasoline injection case that parent parcels have higher momentum than parent parcel of diesel injection case. The speed of gasoline parcel at impingement is increased due to low injection pressure which causes the air resistance didn't sufficiently decrease the droplet momentum. However, the previous Bai model didn't consider the amount of dissipation energy on the whole parcel speed range. The dissipation energy amount is too small to affect total kinetic energy of child parcel. In Bai renewal model, the amount of dissipation energy is determined according to parent parcel velocity. The viscous dissipation due to deformation accounts for around 80% ~ 90% [8]. Thus, it is suggested that the minimum value of the dissipation energy 80% of parent kinematic energy.

$$E_C = max\left(0.8 \cdot (\frac{1}{2} m_I U_I^2), \frac{k}{12} \sigma \pi d_I^2\right) \tag{1.6}$$

The coverage range problem is solved in renewal model. However, the model still assumes that 1-D momentum transfer. Thus, the fuel film shape is symmetric. The tangential velocity of child parcel was determined by model constant. The model constant should be corrected repeatedly. Therefore, researcher experience is important to match rebound spray radius.

1.2.3 Kim model

In bai model, each child parcel has identical mass. Because the number of droplet is determined randomly, the child droplet mass also determined randomly. Thus, in some specific case the child parcel velocity can exceed parent parcel velocity. Kim [9] used experimental data which contain child droplet diameter distribution [10]. Moreover, four child parcels were generated from one parent parcel. 2-D momentum transfer and distribution can be described in Kim's model. There are various momentum sources in spray wall impingement phenomenon. Every momentum source should be considered to describe proper film movement. However, Kim's model assumed that shear force between air and film only affects its movement. The shear force is dominant factor when it is analyzed that Port Fuel Injection (PFI) engine which the speed of air reaches 200 m/s near the intake valve. Therefore, the other factors can be ignored. In DISI engine case, the momentum source which comes from droplet momentum loss is the most significant source. Thus, the interaction between spray and wall affect much part of film movement. In conclusion, the source from spray wall impingement should be adopted to represent spray wall impingement and film formation properly in DISI engines which are mainly used recently.

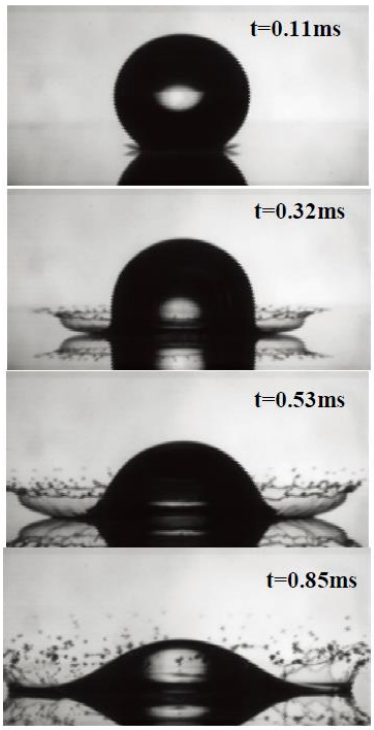

Figure 6. Overall process of splash phenomenon [11]

As shown in figure 5, the splash phenomenon in real situation generate much of the child droplets. To simulate realistic phenomenon, the number of child droplets derived from parent droplet must be increased. Furthermore, the mass of each droplets should be differed. The model should be developed to represent the experimental data which shows much more number of child droplets and more complex behavior.

By using experimental data of child droplet, the Kim's model simulates moderate droplet behavior. However, proper dissipation model is needed to reflect the behavior of real droplet impingement phenomenon.

1.3 Objective

The objective of this work is to improve spray-wall interaction predictability by considering droplet energy dissipation and 2-D momentum transfer in fuel film.

The dissipation amount of droplet energy is increased proportionally to the its kinetic energy. According to bai renewal paper, the droplet dissipation amount is determined within specific range [8]. When the speed of droplet before the collision is over 30 m/s, the dissipation amount which is calculated by weber number and surface tension is not sufficiently large to affect initial kinetic energy. Thus, the dissipation energy should be calculated by considering parent parcel energy when collision speed of parent droplet is above 30m/s such as DISI engine case.

To accurately describe spray wall impingement, 2-D momentum transfer, child droplet properties and behavior should be considered. In this work, the objective is to improve previous model based on above consideration. The number of child parcels derived from parent parcel should be increased to depict 2-D momentum transfer. Then the Rosin-Rammler distribution is used to reflect child parcel diameter.

The modified model is validated with experiments. The Mie-scattering images of iso-octane spray near wall were acquired to measure rebound spray radius and height.

Chapter 2. Wall Impingement Model

2.1 Regime Transition Criteria

When the droplet collides to the wall, the regime criteria should be clarified to simulate. Almost 70% of soot is generated during warming-up. Not sufficient time to warm up engine from low temperature increase local inhomogeneity of air fuel mixture which provide optimal conditions for forming soot. For instance, the mixture near the film goes rich because low wall temperature deters film evaporation. Thus, the rig experiment is progressed under boiling temperature. As a result, droplet behavior is analyzed under boiling temperature. As shown in figure 4, simply limiting the temperature can restrict impingement regime. Strick, Spread, Splash are the regime to consider [3]. When the droplet weber number is increased, the changed droplet movement regime is given below:

(a) Dry wall: Stick → Spread → Splash

(b) Wetted wall: Rebound → Spread → Splash

As the weber number increases, the amount of parent parcel energy increases. Therefore, the child parcel tends to move dynamically. The results of Bai experiments show the stick phenomenon is occurred only We < 1 when wetted wall condition. Thus, stick regime is ignored [3].

2.1.1 Dry Wall

Adhesion (stick/spread)

$$K < 57.7 \tag{2.1}$$

Above inequation is decided by experiment of Mundo [10]. According to Mundo, the experiment results show that surface roughness is not related to splash regime. Thus, the criterion is defined newly.

Splash

$$K > 57.7 \tag{2.2}$$

Splash phenomenon is occurred when K value is above 57.7. Increasing the K value increases the kinetic energy of parent parcel compared to the surface tension energy.

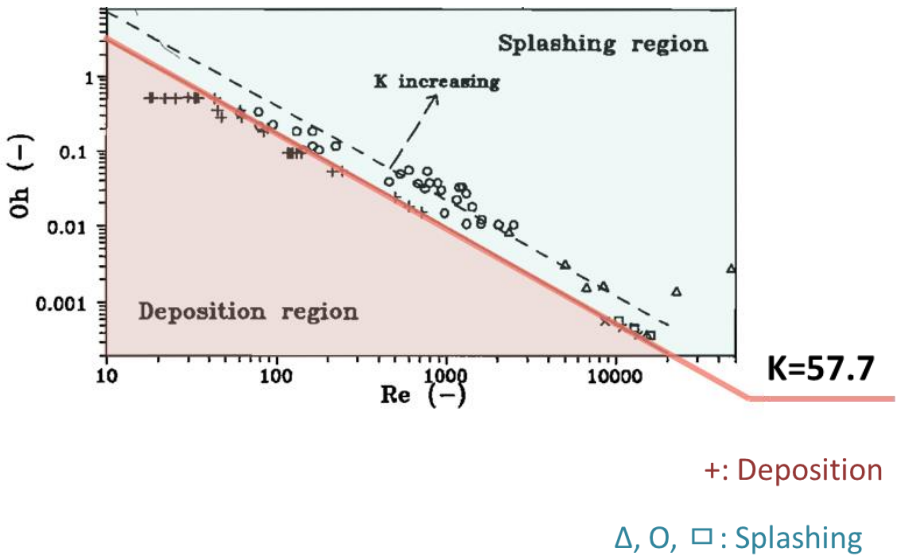

Figure 7. Criteria between splash and deposition regardless plate surface [10]

2.1.2 Wetted Wall

When parent parcel has small We, the rebound phenomenon is observed on wetted surface [9].

$$K < 57.7,\ We < 5 \tag{2.3}$$

The parcel rebound phenomenon is occurred below We number 5. The criteria are determined by the mean of experiments. Also, the experiments show that splash phenomenon occurs in same condition regardless of whether the surface is wet or not. The figure 6 shows that the collision behavior of parent droplet is determined by K. The larger K tend to occur more splash phenomenon. The K criteria between splash and deposition can be selected the value of 57.7.

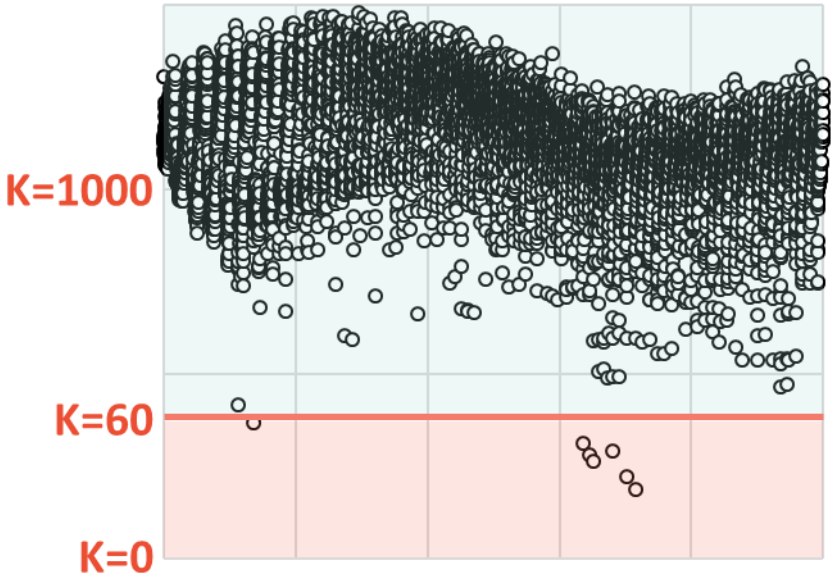

Figure 8. K value of each droplet under typical DISI spray which injection pressure is 150 bar. Droplets are normally in splash regime.

The figure 7 is the calculation results of injected parent droplet with 150 bar. Every single parcel data is acquired by user subroutine of STAR-CD then the value of K is calculated from Reynolds number and Weber number. It shows that almost all the sprayed droplets are splashed in DISI engine due to low injection pressure. Compared to diesel injection, DISI injection has low injection pressure which generates relatively big parent droplet due to restricted atomization effect. The larger size of the droplet, the easier the droplet can maintain momentum.

The splash regime was carefully modified considering that the it is mainly occurred in simulation. The amount of dissipated energy is calculated properly for DISI engine condition which the speed of parent droplet is over 30 m/s. Also, the child droplet velocity is fully calculated by energy equation. It allows the model can offer rigid solution. The diameter of child droplets is determined based on experimental results rather than random distribution. The distribution is simulated by using PDF. Thus, the diameter and velocity distribution of child droplet are more realistic behavior. The number of child droplet derived from parent droplet is increased to simulate 2-D momentum transfer. In addition, the modified model considers shear force, impingement momentum and local pressure difference to describe film movement. Thus, the model covers broader area ranging from the shear force dominant case such as PFI to droplet induced momentum and pressure dominant case such as DISI.

2.2 Impingement Modeling

2.2.1 Adhesion

When adhesion is occurred, the droplet momentum is fully converted to film momentum source. Parcel momentum and energy are converted into pressure and momentum and applied to the equation as source term. The equations are introduced in film modeling section.

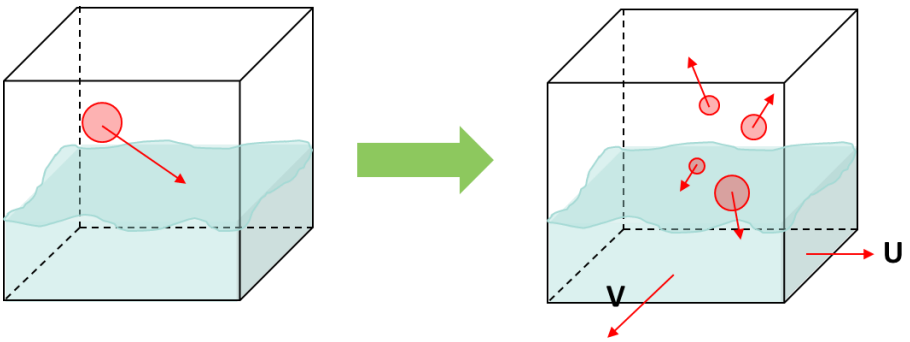

Figure 9. Schematic description of impingement phenomenon

The figure 8 can describe overall momentum and energy transfer of every cases. In the case of adhesion, child parcels are not generated and every property go to film. Next, some of the parent parcel properties go to film then rest of them go to rebounded parcel in rebound model. At last, the child parcels are generated in splash model. The properties of parent parcel are transferred to both child parcels and films. Moreover, each child parcel has different properties which follow experimental distribution.

2.2.2 Rebound

The parent parcels movement are described to rebound when the Weber number is below the 5 and the K is below the 57.7. on the wet surface. In the case of parcel rebound, velocity of the parcel is determined by the equation based on Matsumoto [12] experiment which is described by equation (2.4) ~ (2.6).

$$u_d' = \frac{5}{7} u_d^0 \tag{2.4}$$

$$v_d' = -e v_d^0 \tag{2.5}$$

$$e = 0.993 - 1.76\theta_I + 1.56\theta_I^2 - 0.49\theta_I^3 \tag{2.6}$$

The velocity of child parcel is decreased by wall friction, droplet deformation, and momentum transfer to film. The restitution coefficient e is based on results of Grant [13]. $\theta_I$is incoming angle of attack which is expressed by radian. In addition, the rebound parcel direction retains its parent parcel direction. The dissipated momentum is assumed that it goes to film. It is applied to the film momentum equation as used in adhere section.

2.2.3 Splash

To imitate splash phenomenon, it needs to be simplified through reasonable assumptions. It is assumed that a parent parcel collides to wall, four child parcels are generated [9]. The previous model assume two child parcels are generated from collision [3]. Thus, there is a limitation that film transferred momentum is described only 1-D. In this work, to consider 2-D spray-wall impingement phenomenon more accurately, the number of child parcels derived from the parent parcel is increased from two to four. Thus, rebound spray radius and height are well simulated.

The other assumption is that a parcel includes many droplets [14]. Due to limitation of computing power, parcel concept is adopted to the simulation. Concept diagram is given in figure 9. Every droplet in a parcel has the same diameter. Because of mass conservation, the number of the droplet could be rational number. In conclusion, although the parcel has physical properties based on droplet diameter, it has total mass of droplets in single parcel.

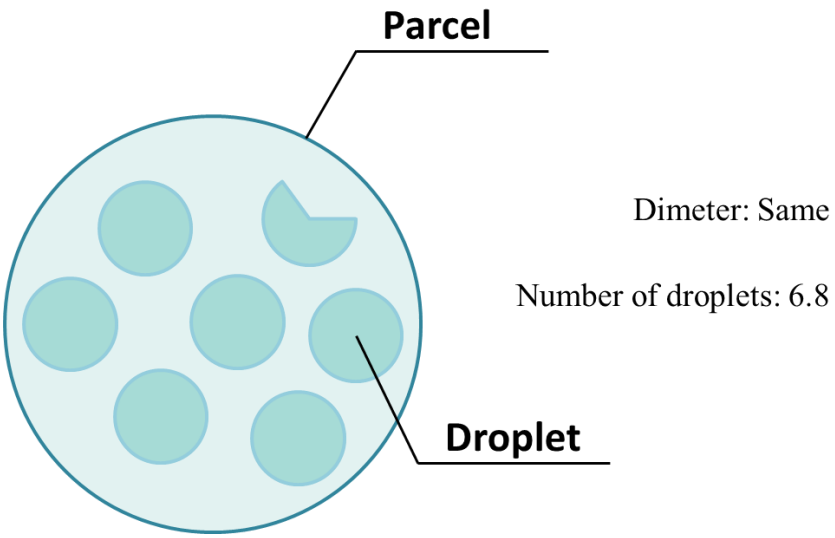

Figure 10. Concept diagram of a parcel which has 6.8 identical droplets.

In simulation, the mass of child parcels are based on experiment data of stow [15] and Levin [16]. Also, the diameter of child parcel is determined by data from child droplet behavior observing experiment of Mundo. The distribution of child droplet diameter is captured by using a Probability Density Function.

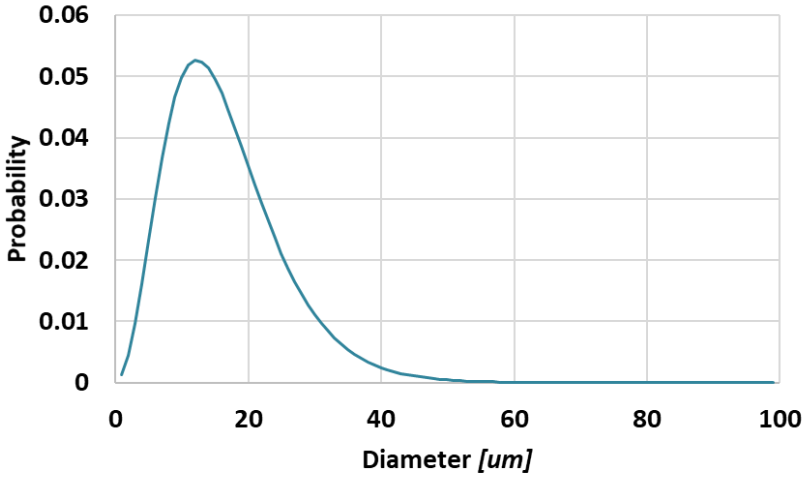

Figure 11. PDF of child droplet diameter

The sum of each child parcels mass is determined by equation 2.7 [3].

$$r_m = \frac{m_s}{m_I} = \begin{cases} 0.2 + 0.6\alpha, for\ dry\ wall \\ 0.2 + 0.9\alpha, for\ wetted\ wall \end{cases} \quad (2.7)$$

α is random number which is distributed uniformly 0 ~ 1. The range of mass ratio differ in accordance with surface. The mass ratio can be over 1 after splash on the wet surface. These results are observed by Mutchler [17].

It is assumed that each parcel has same mass. Mass conservation equation is given by equation (2.8).

$$N_1 d_1^3 + N_2 d_2^3 + N_3 d_3^3 + N d_4^3 = r_m d_I^3 \quad (2.8)$$

N_1, N_2, N_3, N_4 are the number of droplets in each parcel, d_1, d_2, d_3, d_4 are the mean diameter of each child droplet in the parcel. d_I is the diameter of droplet in parent parcel.

Energy conservation equation is given by equation (2.9).

$$r_m \cdot \left(\frac{1}{2} m_I U_I^2 + \pi\sigma N_I d_I^2 - \frac{K}{12}\pi\sigma d_I^2\right) \tag{2.9}$$
$$= \frac{1}{8} m_S (U_1^2 + U_2^2 + U_3^2 + U_4^2) + \pi\sigma (N_1 d_1^2 + N_2 d_2^2 + N_3 d_3^2 + N_4 d_4^2)$$

The total parent parcel energy consists parent parcel kinetic energy and sum of each droplet surface energy. When the parent parcel collides to the wall, critical kinetic energy and child parcels surface energy are subtracted from total parent energy. The critical kinetic energy is the minimum energy when the parcel starts to splash. It is expressed by function of Weber number and surface tension and means deformation, dissipation energy of parent parcel and liquid film transferred energy [3].

According to bai renewal model, when the high-speed collision occurs in DISI engine, the droplet kinetic energy is too large to reduce meaningful amount by weber number and surface energy. From phenomenological analysis, the difference between incoming kinetic energy and critical kinematic energy do not exceed 0.2 incoming kinematic energy [18]. As a result, the critical energy should be modified by equation (2.10) in specific case.

$$E_C = max\left(0.8 \cdot \left(\frac{1}{2} m_I U_I^2\right), \frac{k}{12}\sigma\pi d_I^2\right) \tag{2.10}$$

Finally, the remainder of energy go to net child parcel kinetic energy.

Velocity ratio of each parcels are decided by equation (2.11) which is suggested by Ghadiri [19].

$$\frac{u_i}{u_j} = \frac{ln\left(\frac{d_i}{d_I}\right)}{ln\left(\frac{d_j}{d_I}\right)} (\mathrm{i,j} = 1 \sim 4, \mathrm{i} \neq \mathrm{j}) \tag{2.11}$$

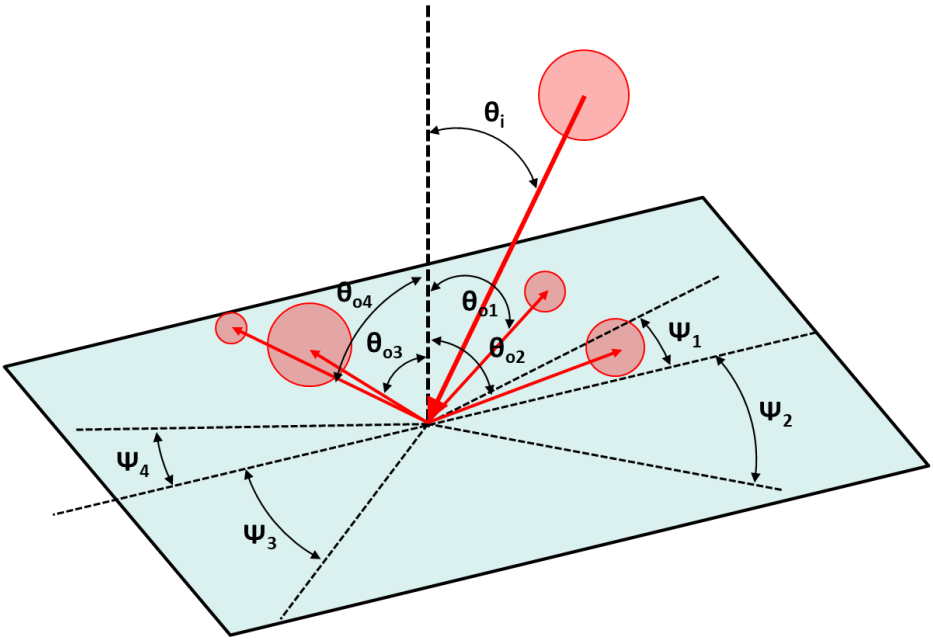

Figure 12. Schematic diagram of splash phenomenon

The child parcels direction is determined based on experimental data [10]. According to Mundo investigation, angle between child droplet direction and wall normal vector is determined by equation (2.12).

$$\theta_o = 70 + 0.25\theta_i \pm 10 \cdot Random \tag{2.12}$$

The azimuth of the each parcel(ψ) is arbitrarily determined between 0 and 30.

2.3 Film Modeling

2.3.1 Mass Continuity

The film mass source comes from spray wall impingement. The remainder which is calculated from equation (2.7) transfer to fuel film. The number of colliding parcel is counted during one iteration. After that, the summation of remainder is adopted as Dirac delta function to mass conservation equation. The mass conservation equation is given by

$$\frac{\partial \rho\delta}{\partial t} + \nabla \cdot (\rho\delta U) = S_{\rho\delta} \tag{2.13}$$

$S_{\rho\delta}$ is source term which can be divided in to the equation (2.14) [20].

$$S_{\rho\delta} = S_{\rho\delta,imp} + S_{\rho\delta,splash} + S_{\rho\delta,vap} + S_{\rho\delta,abs} + S_{\rho\delta,sep} \tag{2.14}$$

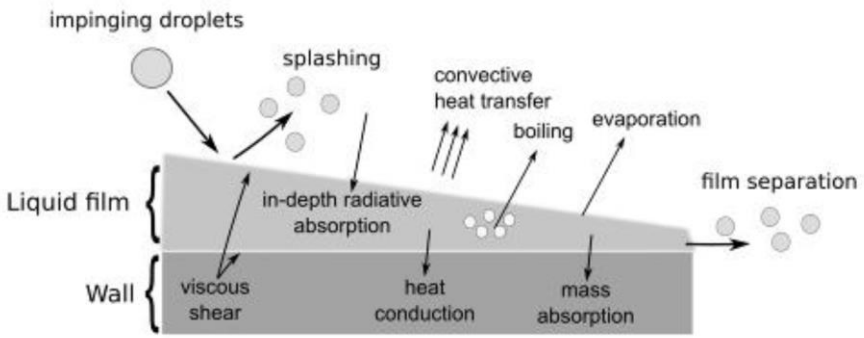

Figure 13. The detail description of interaction between droplet and film [20]

Among the source term which is presented above, the most dominant parameters are impingement and splash term which is presented by equation (2.15).

$$S_{\rho\delta(imp,spl)} = \frac{\Sigma m_{(imp,spl)}}{A\Delta t} \tag{2.15}$$

The cumulative mass on each cell is calculated and adopted to source term. Low surface temperature, impenetrable media, and smooth surface are provided in engine cold start condition. Due to surrounding environment, the spray wall impingement phenomenon is prominent.

$S_{\rho\delta,vap}$ means specific evaporation rate. This term is defined as a function of film surface area which loss can be calculated by energy equation.

$S_{\rho\delta,abs}$ means film absorbed amount by the porous surface. The absorbing phenomenon is important to treat fire equipment such as sprinkler because most of the combustibles has porous surface. However, it is negligible in engine condition.

$S_{\rho\delta,sep}$ means detached droplet amount from surface film such as intake valve

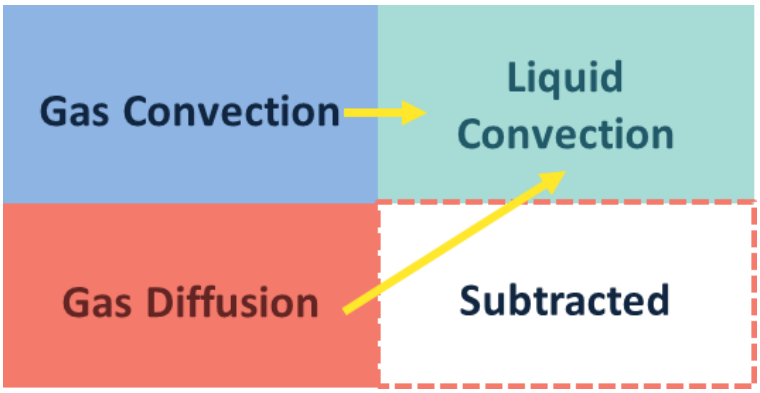

Figure 14. The schematic diagram of mass continuity

2.3.2 Momentum Continuity

Film momentum is transferred through two main components. They are pressure and momentum source. Because total momentum should be conserved, the film momentum and child parcel momentum always have same value of parent parcel momentum. Furthermore, the local difference in pressure which come from spray impingement generate film momentum. The magnitude of pressure and momentum source are calculated in the same way of mass continuity. The number of parcel which transfer film momentum and create pressure is counted in each time step. Then the amount of them are adopted as Dirac delta function to momentum equation.

Momentum equation is described by equation (2.16).

$$\frac{\partial \rho \delta U}{\partial A} + \nabla \cdot (\rho \delta U^2) = -\delta \nabla P + S_{\rho \sigma U} \tag{2.16}$$

Momentum source term and pressure source term can be specified by a few terms.

$$P = P_{imp} + P_{spl} + P_{vap} + P_{\sigma} + P_{\delta} + P_g \tag{2.17}$$

The key parameter P_{imp}, P_{spl} can be expressed as presented by equation (2.18).

$$P_{(imp,spl)} = \frac{\Sigma(m_{(imp,spl)} \cdot v_{n(imp,spl)})}{A \Delta t} \tag{2.18}$$

There are bunch of pressure terms. However, it is too small to affect film movement except the impingement and splash pressure in cold engine condition. At the edge of the film, the capillary force should be considered to clarify boundary. However, the effects of capillary force are reduced in the middle of

the film.

P_{vap} is evaporation pressure due to film evaporation, the evaporation pressure is related to evaporation rate and density of gas phase film. It is increased in proportional to gas phase density and surface-normal velocity of the vaporizing gases.

P_{σ} is Capillary pressure. Surface tension and curvature are main parameter of capillary pressure. When the curvature is small, capillary pressure can be expressed as equation (2.19).

$$P_{\sigma} = -\sigma \nabla^2 \delta \tag{2.19}$$

P_{δ} is hydrostatic pressure which can expressed as equation (2.20).

$$P_{\delta} = -\rho(n \cdot g)\delta \tag{2.20}$$

P_g is Local gas pressure which is the pressure near the liquid film.

$S_{\rho\delta U}$

$$= \tau_g - \tau_w + \tau_{mar} + \rho g_t \delta + F_{\theta} + S_{\rho\delta U,imp} + S_{\rho\delta U,spl} \tag{2.21}$$

τ_g, τ_w are shear stress which represent film-gas and film-wall respectively. Normally the shear stress between film and wall is dominant. However, the shear force between film and gas could be increased to nearly the same level, if specific conditions are met. For instance, it is important in port injection case due to the velocity of air fuel mixture near intake port is above 100m/s.

It should be assumed that the velocity profile of liquid film is parabolic in the wall-normal direction. The velocity profile assumption remains valid for laminar and wavy laminar film flows [21]. The film can be described as laminar

below the value of Re<900 [22]. The engine spray case normally under the laminar condition. Thus, the shear force easily calculated from assumption.

τ_{mar} is thermocapillary stress. The local temperature difference is main factor of surface tension difference. It is also called Marangoni effect. The local temperature gradient cause surface tension variations which is inversely in proportional to temperature. The thermocapillary stress tend to drive the fluid from low surface to high surface region. In the other words, it acts from hot regions to cold regions. It is dominant when the surface temperature is sufficiently high [23]. When the engine condition is simulated, the Marangoni effect should be considered.

F_θ is contact angle force. Surface tension is main inducing parameter of contact angle force at the end of film. The surface tangential force limits the film from spreading. When the film flow on inclined surface, the contact angle force is dominant factor to determine the wetted flow behavior such as rivulets. The film will not able to flood the surface to near cells below the critical film radius. The specific calculation method is given equation (2.26) ~ (2.30). The detail description of critical film radius is given in [24]

.

The predominant factor of momentum source also related to impingement and splash. The factor $S_{\rho\delta U,imp}$, $S_{\rho\delta U,spl}$ are can be expressed as equation (2.22).

$$S_{\rho\delta U}{}_{(imp,spl)} = \frac{\Sigma(m_{(imp,spl)} \cdot v_{t(imp,spl)})}{A\Delta t} \tag{2.22}$$

The momentum from parcel should be divided into cell side normal directions. Then amount of source per unit area in each time step is calculated and adopted to film momentum continuity equation. The Dirac delta function is likewise used.

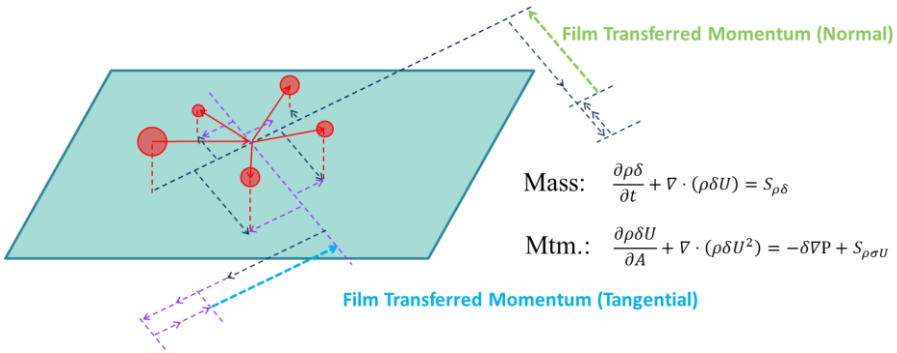

Figure 15. The amount of film momentum transfer from splash

In this paper, to consider 2-D spray-wall impingement phenomenon more accurately, the number of child parcels derived from the parent parcel is increased from two to four. The more detailed tangential momentum source can be expressed. Tangential momentum sources which are aligned to droplet velocity direction and normal to droplet velocity direction are successfully adopted to spray wall impingement model.

2.3.3 Energy Continuity

Because of no chemical reaction and low surface temperature, there is no big difference between parent parcel and child parcel. Thus, energy transferred amount to film is almost nonexistent except for enthalpy which come from mass. Energy equation is described by equation (2.23).

$$\frac{\partial \rho \delta h}{\partial t} + \nabla(\rho \delta U h) = S_{\rho \delta h} \tag{2.23}$$

Separated energy Source Term is given by equation (2.24).

$$S_{\rho gh} = \dot{q}_g'' + \dot{q}_w'' + S_{\rho gh,vap} + S_{\rho gh,imp} + S_{\rho gh,spl} + S_{\rho gh,abs} \tag{2.24}$$

$\dot{q}_g''$ is convective heat transfer amount from gas.

$\dot{q}_w''$ is convective heat transfer amount from wall.

$S_{\rho gh,vap}$ is energy source term due to evaporation. It can be expressed by vaporization rate and latent heat. The vaporization rate below the boiling point is in proportional to difference between vapor fraction of interface and ambient statement. The vaporization rate is affected by energy equation, not concentration gradient above the boiling temperature. The specific calculation methods are presented in [14].

The key parameters are $S_{\rho gh,imp}$, $S_{\rho gh,spl}$ which are from impinging spray.

$$S_{\rho \delta U}{}_{(imp,spl)} = \frac{\Sigma(m_{(imp,spl)} \cdot h_{(imp,spl)})}{A \Delta t} \tag{2.25}$$

$S_{\rho gh,abs}$ is expressed by absorption rate and enthalpy of the absorbed liquid like vaporization.

Except added enthalpy from impingement, the effect of evaporation and

condensation calculated by heat transfer. The film evaporation amount is related to magnitude of latent heat. The latent heat is difference between gas conduction and liquid conduction.

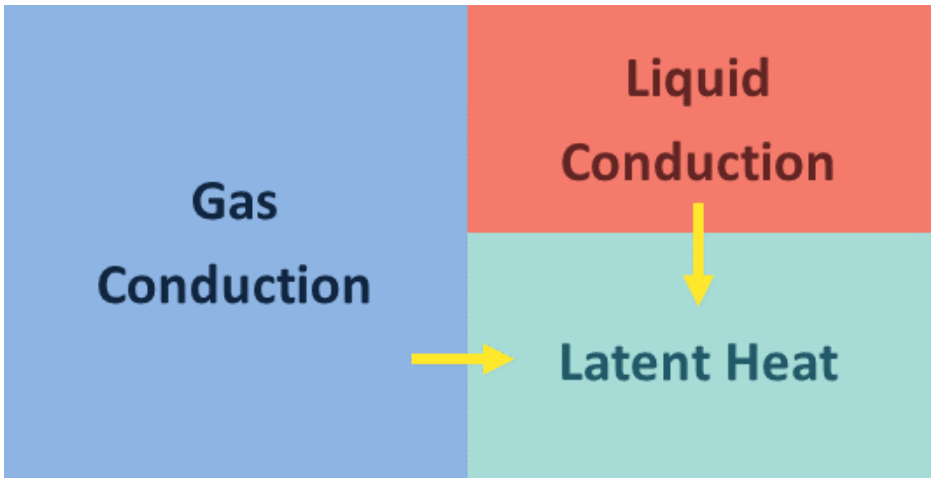

Figure 16. The schematic diagram of energy continuity.

2.3.4 Film Movement Criterion

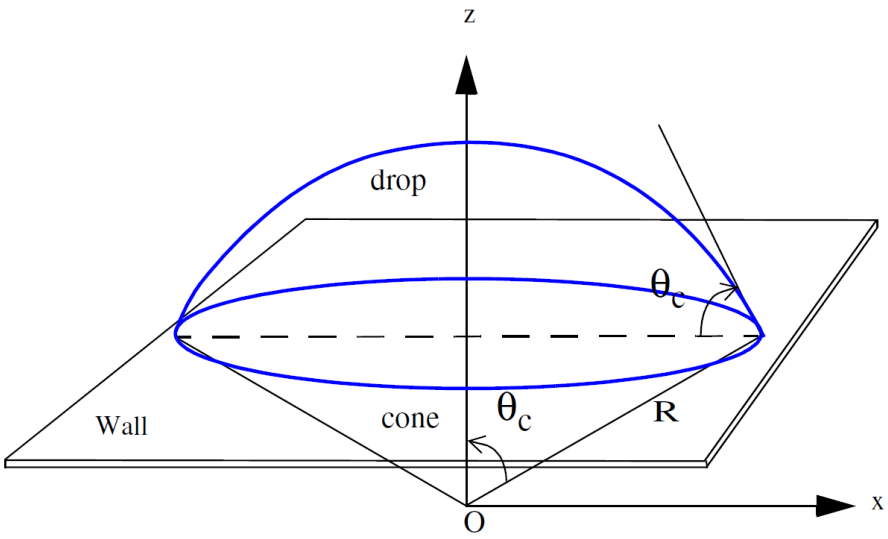

Figure 17. Definition of critical radius of droplets on the horizontal plane [14]

The film is considered as continuous flow. Therefore, the criteria should be determined to prevent continuous flooding problem. Whether the surface is wet or not at the edge of the film is determined by critical radius. If the film radius is larger than critical radius, the film moves to near cell and the boundary is expanded. The critical radius can be defined by its volume.

$$V_g = \frac{2}{3}\pi R^3 f(\theta_c) \tag{2.26}$$

$$f(\theta_c) = 1 - \cos\theta_c - \frac{1}{2}(\sin\theta_c)^2 \cos\theta_c \tag{2.27}$$

The film at the edge is assumed that it shaped sphere. At the end of the edge, the contact angle exists. The contact angle is related to its surface tension, capillary pressure, density, surface roughness, etc. The net force can be calculated from contact angle. When contact angle is considered as constant,

the critical radius can be determined as shown by equation (2.28) ~ (2.30).

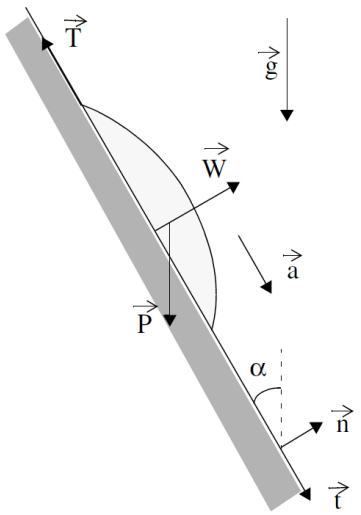

Figure 18. Forces acting on droplet on an inclined wall

The motion equation can be formulated with force of gravity, normal force, surface tension. They are described on figure 16.

$$P + W + T = m_g a \tag{2.28}$$

$$P = \rho \frac{2}{3} \pi R^3 f(\theta_c) g \tag{2.29}$$

$$T = -2\pi\sigma R \sin\theta_C (1 - \sin\theta_C) t \tag{2.30}$$

Finally, the critical radius is expressed by equation (2.31).

$$R_c = \sqrt{\frac{3\sigma \sin\theta_c (1 - \cos\theta_c)}{\rho f(\theta_c) \left(g \cos\alpha + \frac{v_f}{\Delta t} \right)}} \tag{2.31}$$

$R < cR_c$: Film adheres to the wall.

$R > cR_c$: Film continues to move.

When the radius is less than critical radius, the film adheres on the same cell. However, the radius of the film edge cell is greater than critical radius the film is move to near cell. Because the contact angle has different value on the same surface in different condition, the model constant is adopted. Film speed, rivulet width, and heat transfer rate representatively affect contact angle [7].

Chapter 3. Experimental Setup

An experiment was conducted to compare and validate models by Istituto Motori [25]. Mie scattering and Schlieren method using LED and Camera is conducted to capture spray wall impingement phenomenon. Both technics well captured the spray-wall impingement phenomenon. The specific setups are given on figure 18. Then the specific conditions are given on the table 1.

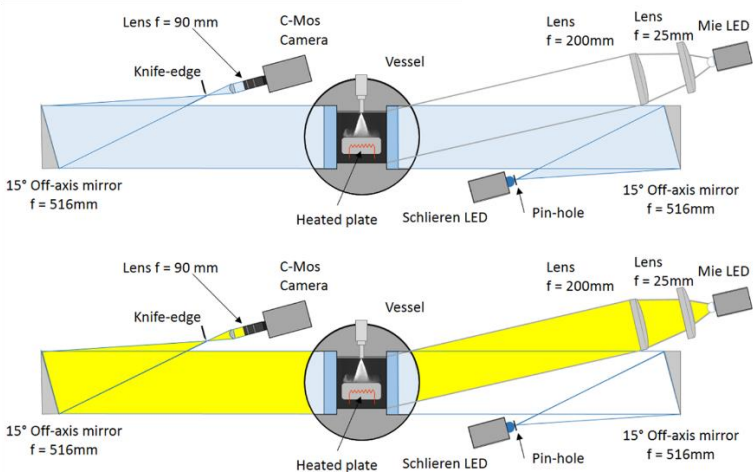

Figure 19. Quasi-simultaneous Schlieren and Mie scattering techniques

Table 1. Experimental Condition

Specification	
Fuel	Iso-octane
Injection Pressure	15.0 MPa
Injector hole diameter	0.2 mm
Wall Temperature	295 K
Vessel temperature	295 K
Fuel temperature	300 K

3.1 Injector and Vessel Specification

The DISI injector has axially-disposed single-hole which hole diameter is 200μm as well as the static flow rate is 2.45g/s at the injection pressure of 10MPa. A pneumatic injection system pressurized the fluid up to 30.0MPa and fed the injector. ECU and the acquisition systems matched each other by external TTL signal. A cooling cup and J-type thermocouple which has very thin diameter to achieve fast response are mounted very close to injector exit hole to control the injector temperature. The thermocouple was allocated in a grove on the external of the injector body. In this study, the iso-octane was used as injecting fluid to avoid problems arising the nature of the multi component fuel. The fuel temperature was kept at 300 K.

The constant volume high-pressure vessel which has three orthogonal quartz windows is used to access the investigated area. The vessel was kept at room temperature and atmospheric ambient pressure. The aluminum flat plate with a diameter of 80mm positioned 26 mm below the injector tip which is facing orthogonal to the spray axis in the chamber. The average roughness of the wall is 1.077μm, measured by the Stylus Profilometer, Model Surtronic 3 by Rank Taylor Hobson. The plate was heated to 295K by electric resistances and controlled in temperature by a J-type thermocouple equipped in its center below 1.0 mm from the wall surface. A Watlow series 985 thermostatic system controlled the temperature in the range of ± 1 °C. The detailed description of the experimental setup for injector and constant volume vessel are provided in [26].

3.2 Hydraulic Properties

AVL fuel injection rate meter working on the Bosch tube principle was used to measure injector properties [27]. 1.0ms of the nominal energizing current signal which is 1.3ms effective discharge 2.53, 3.47, 4.19, and 4.84 mg/shot of fuel at the injection pressures of 5.0, 10.0, 15.0, and 20.0MPa, respectively.

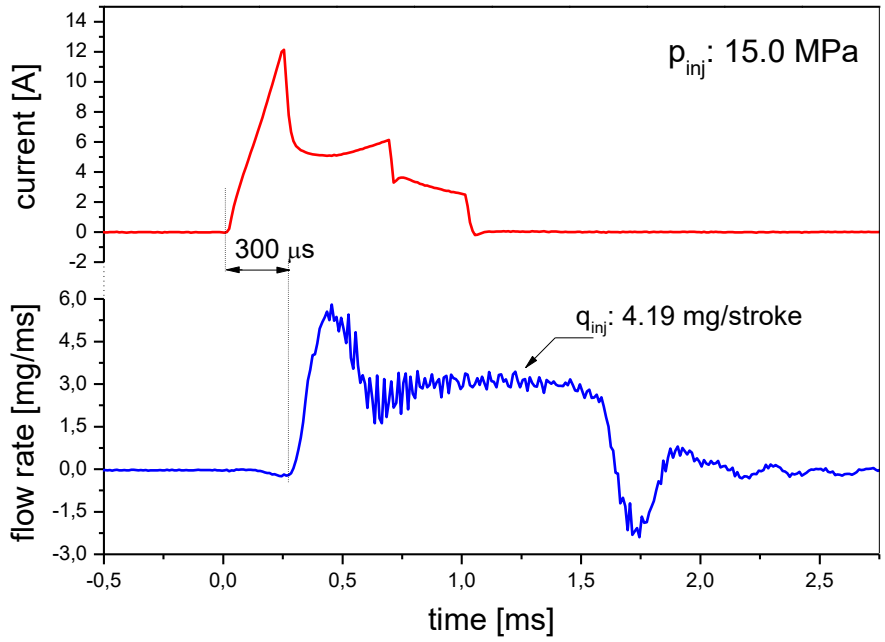

Figure 20. Solenoid energizing current and fuel injection rate

The link between the solenoid energizing current profile (top) and the corresponding fuel injection rate (bottom) measured by the AVL meter at the injection pressure of 15.0MPa for 1.0ms energizing are shown above figure. A 300μs delay is observed between the activation of the electronic signal and the

real start of the injection event. The injected quantity is the integral of the profile along the pulse duration. The total amount of injected fuel is equal to 4.19 mg/stroke. The opening over shoot in the energizing currents lead mass flow rate profile shows an initial peak, while dumped oscillations arise because of fluid dynamic effects in the Bosch tube at the end of injection.

3.3 Optical Diagnostics

A combined Z-type Schlieren and Mie scattering optical setup was used to investigate the impinging spray analysis by varying the wall temperature. Using the same optical path allow to acquire Schlieren and Mie scattering images quasi-simultaneously. This methodology complement Mie scattering technic which capture the liquid phases of the spray by comparing with Schlieren which collect the liquid/vapor ones for determining both the phases. The time differences between the Mie scattering and Schlieren is around 20μs. Thus, negligible differences appear in the penetration of the leading edges. Further details on the wall-injector configuration in the vessel were offered in [28]. A blue high-speed LED which has 455nm/450mW was used as light source for Schlieren image. A collimated beam which is generated by a first mirror illuminate the spray. A second mirror focused the image on a razor blade which placed horizontally to the first mirror. Then the image is set on a high-speed C-Mos camera (Photron FASTCAM SA4) by a 200mm focal spherical lens. The Mie-scattering arrangement was in forward and having its axis a displacement angle of 5° with respect to the Schlieren one. The high-speed C-Mos camera which is synchronized with the injection system was utilized to acquire alternatively both the Schlieren and Mie scattering images quasi-simultaneous mode. The camera was equipped with a 90mm objective realizing a spatial resolution of 8.47 pixel/mm.

The impinging spray images showed both intact liquid core sprayed from the tip and flowing along the surface of the wall. However, the complex physics

are affect the spray behavior. For instance, the momentum of center droplet in the spray plume is higher than outer droplet, and the lower part of child droplet slide faster than upper part of the splashed droplet, simultaneously the droplets collide to the wall and each other. The figure to aid comprehension are provided on figure 20.

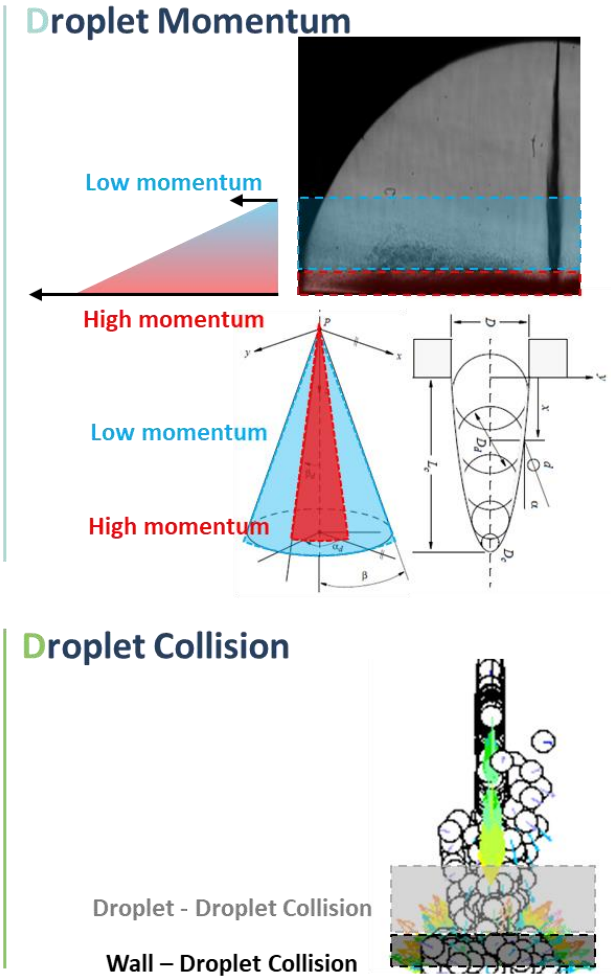

Figure 21. Schematic description of complexity of impingement phenomenon

Therefore, the statistical analysis allows comparing overall shape and validating wall impingement model. Maximum elongation of spray plume sliding along the surface is a function of the time from the impact. The maximum distance from the spray targeting on the surface is called “Rebound spray radius”. The thickness of the intact liquid on the plate has irregular shape, we refer to its maximum height from the plate as to “Rebound spray height”. The liquid core is surrounded by an area composed of fuel vapors mixture. It extends itself on the plate beyond the liquid phase parameter. These parameters can be achieved by comparing Mie scattering and Schlieren image. This area is related to time, wall temperature. and the injection pressure. The criteria of the liquid core and the vapor phase was selected by applying image customized algorithm of processing developed in C#.Net [29]. To get better boundary of both vapor and liquid phase, several procedures are applied on the Schlieren and Mie scattering spray images. Background subtraction, gamma correction, morphology filtering and threshold filtering were applied in sequence. Finally, an automatic procedure extracted the trends of the width and thickness values as function of the injection pressure and wall temperature. A set of 5 images is collected for each injection condition to analyze statistical parameter such as cyclic deviation.

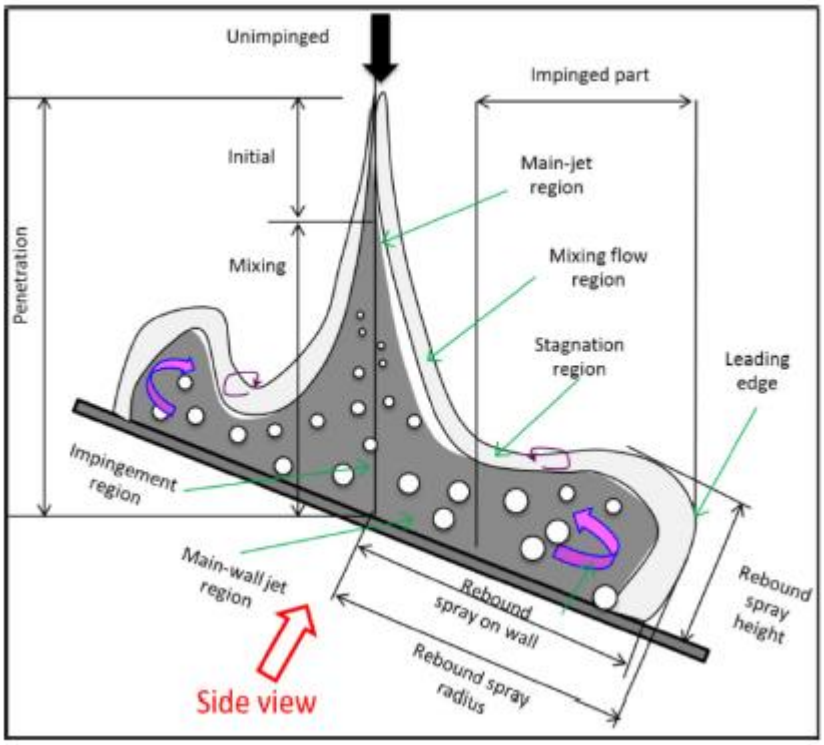

Figure 22. Definition of spray wall impingement parameters [30]

Chapter 4. Simulation Setup

4.1 Computational Domain

The commercial CFD cod STAR-CD v4.22 was used. The experimental environmental was modeled as a three-dimensional box chamber which has 80 x 40 x 26 mm (D x W x H) dimension. Overall, the mesh size is 1 x 1 x 1 mm. However, the neighboring area where collision occurred was refined gradually. Thus, the number of total cell is 97,200. The injecting point is located at (0.05, 0.05, 25.95). It is slightly out of the center to avoid interfere between droplets and cell. All the surface is regarded as non-porous smooth surface and adiabatic condition to ignore wall heat transfer effect. The simulation was carried out based on the Lagrangian multi-phase treatment. The initial temperature field is assumed as constant temperature of 296K. The temperature of injector was maintained at 300K. It has 200um hole diameter and 2.615 outer cone angle. The iso-octane used for experiment was simulated as injecting material. The NIST table was used for the fuel properties. Then the injection rate data which was captured by AVL fuel injection rate meter was put. The number of parcels are controlled to take sake of computational efficiency. 1 million parcels are generated every second.

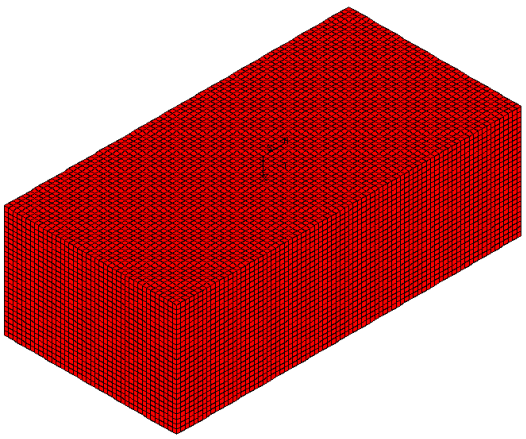

Figure 23. Computational domain

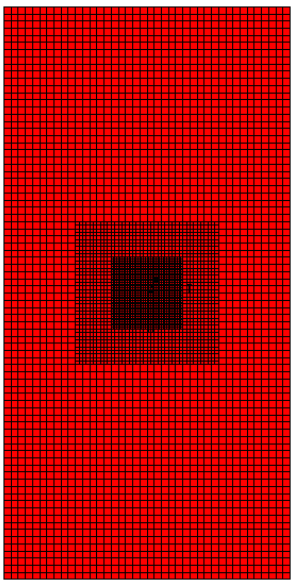

Figure 24. Bottom view of refined domain

4.2 Model Description

The k-ε RNG turbulence model was adopted for turbulent flow [31]. The turbulence interaction between randomly-varying flow field and droplet trajectory was modeled by a stochastic approach [32]. The droplet evaporation and boiling were considered for mass and heat transfer while the condensation was omitted due to the high temperature of plate and environment. The spray is initialized by explicitly defined parcel injection mode. The diameter of parcel follows Rosin-Rammler distribution. The droplet inter-collision follows the O'Rourke model [33] with Nordin constraint [34]. The free spray characteristics like penetration length, spray cone angle were validated with the experimental data by Mie-scattering technique.

Table 2. Model Specification

Models Setting	
Turbulence	k-ε RNG model
Droplet Initialization	Explicit Defined Parcel Injection
Droplet Inter-Collision	O'Rourke, Nordin constraint
Wall Impingement	Kim, Bai
Film	Kim, Bai

Chapter 5. Experiments and Simulations Results

5.1 Wall impingement model

The experiments are conducted with 150bar injection pressure and 295K wall temperature. Simulation results are also gained with same condition. However, the models to simulate phenomenon are adopted differently. The side view of Schlieren image and simulation results are given on figure 24.

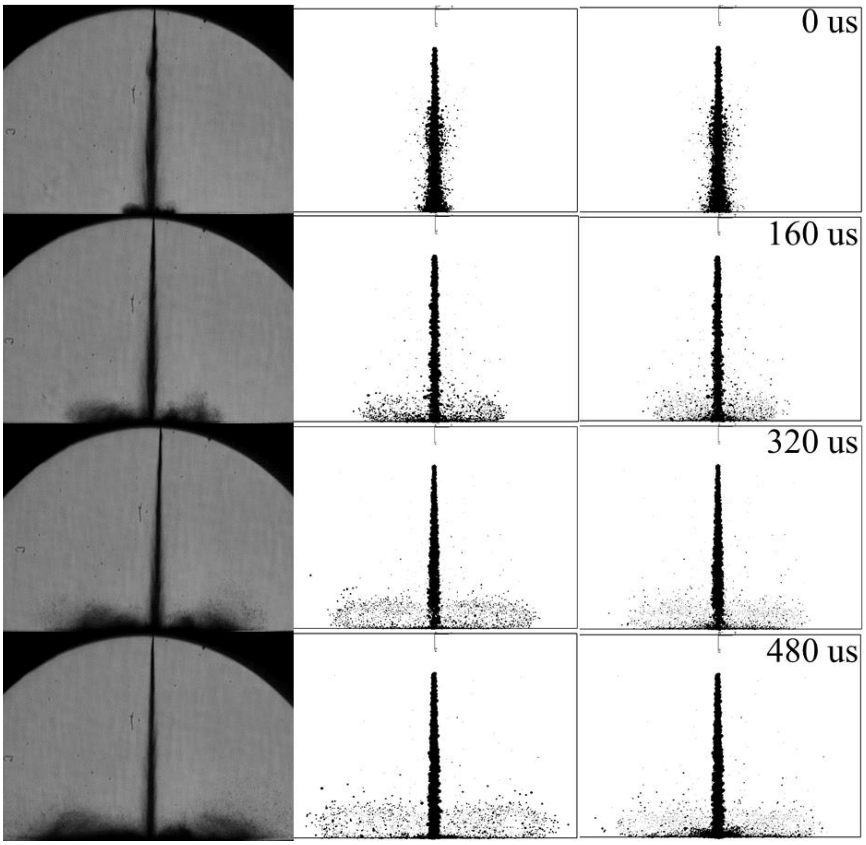

Figure 25. Side view of measured Schlieren image(left), predicted droplet distribution by Kim model(middle), and Bai model(right)

Overall, the shape simulated by Kim model shows better agreement with Schlieren data than Bai model. The rebound spray radius of Kim model is 18% broader than bai model. It means that the tangential component of the child droplet energy in Kim model is larger than Bai model. Likewise, the normal component of the child droplet energy in Bai model is larger than Kim model. Thus, the rebound spray height is 5% higher than Kim model. It is over predicted when It is compared to Schlieren image. The difference is come from tangential velocity determination method. The Kim model determine tangential velocity considering energy equation, however the Bai model simulate the tangential velocity based on model constant. Thus, the only experienced researcher can simulate Bai model properly.

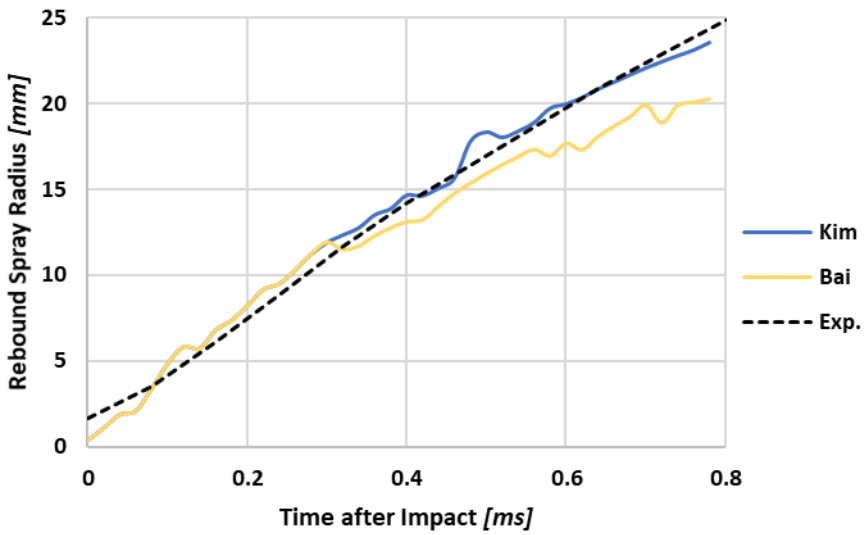

Figure 26. Evolution of rebound spray radius according to time difference

The Kim model shows the best agreement with the experimental results without case-dependent changes to the model constant, when compared to the existing models. The root mean square of difference between Kim model and experiment is 0.56mm. However, the root mean square of Bai model is 3.08mm. The results show that the Kim model has 5 times better accuracy than Bai model. While the two models have slight difference before 0.3ms, the definition of rebound spray radius would cause this phenomenon. The radius is determined by 90% of total spray volume to avoid error from specific overact parcels. As the figure 27 shows the top view of results, the initial difference is not remarkable. However, the spray radius is well matched with experimental data as time goes by.

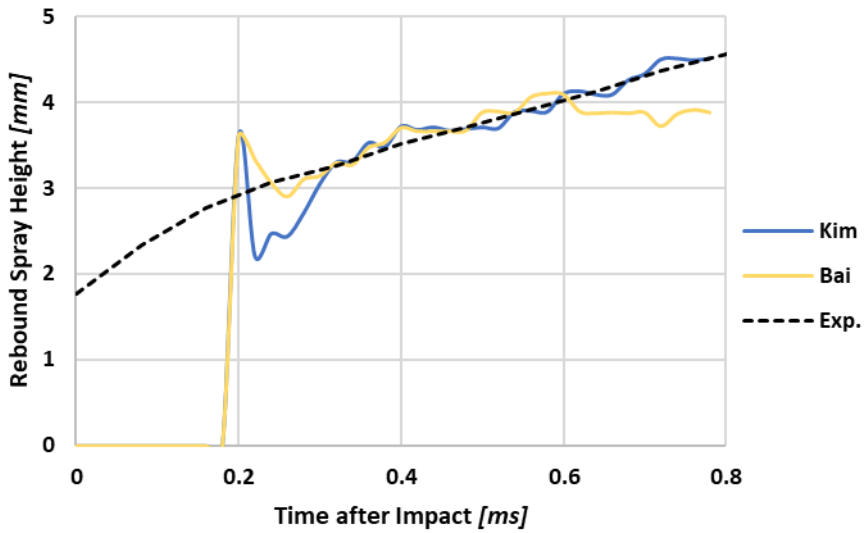

Figure 27. Evolution of rebound spray height according to time difference

Considering the rebound spray radius shows initial error before 0.3ms, the height difference between Kim model and experimental data come from definition. The rebound spray height also be calculated by 90% of total volume faction. Initial silence before overshoot phenomenon and underestimation after overshoot should be modified to change definition of rebound spray height. Another definition is needed to validate both of rebound spray radius and height by considering the experimental data acquiring method. However, after 0.3ms the Kim model shows best agreement with experimental data thanks to modified amount of energy dissipation and child parcel diameter based on experimental data.

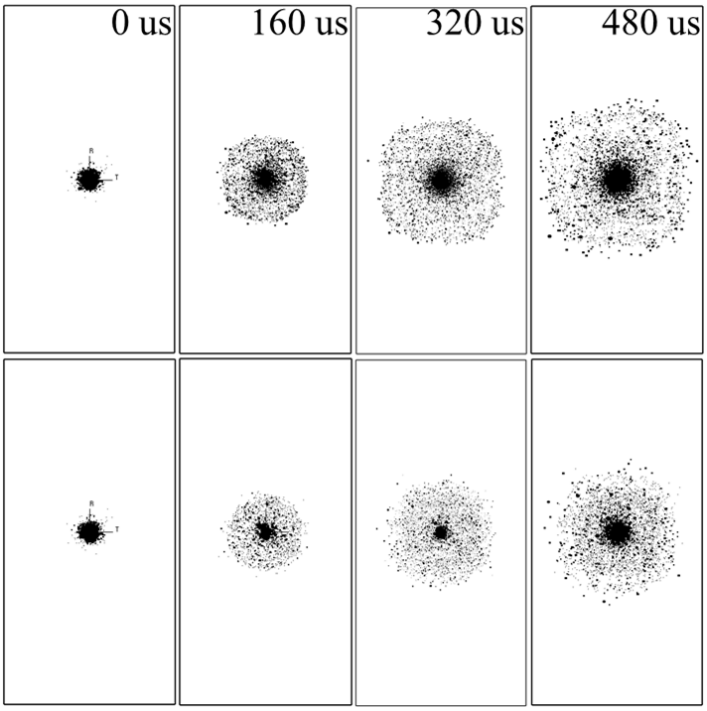

Figure 28. Top view of simulation result by Kim model(top),
and Bai model(bottom)

As described in figure 27, also the rebound spray radius of Kim model is 18% broader than Bai model. Moreover, the modified model allows reasonable distribution of child droplet diameter by using PDF of Mundo experiment. In Bai model, the child droplet diameter is evenly distributed between specific range. Thus, it predicts too much number of smaller droplet which has move faster than average. Even worse, it causes fatal errors that predicts the speed of droplets is faster than the parent droplets.

The figure 28. offers the side velocity plots of two model. The figure shows the child droplets in Bai model have higher normal velocity and take a form of reach an altitude. The remainder of total kinetic energy except the tangential energy which is determined by model constant cause the overestimation tendency. Thus, bai model allows the high normal velocity of child droplets. However, the kinetic energy of child droplets is dissipated and they have reasonable velocity in Kim model. Thus, rebound height of Bai model is much higher than Kim model.

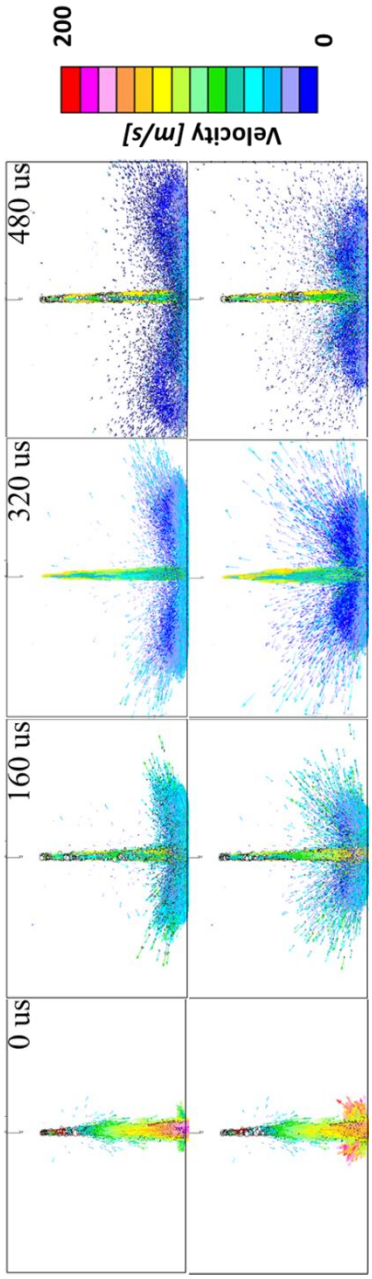

Figure 29. Side view of velocity plot by Kim model(top),

and Bai model (bottom)

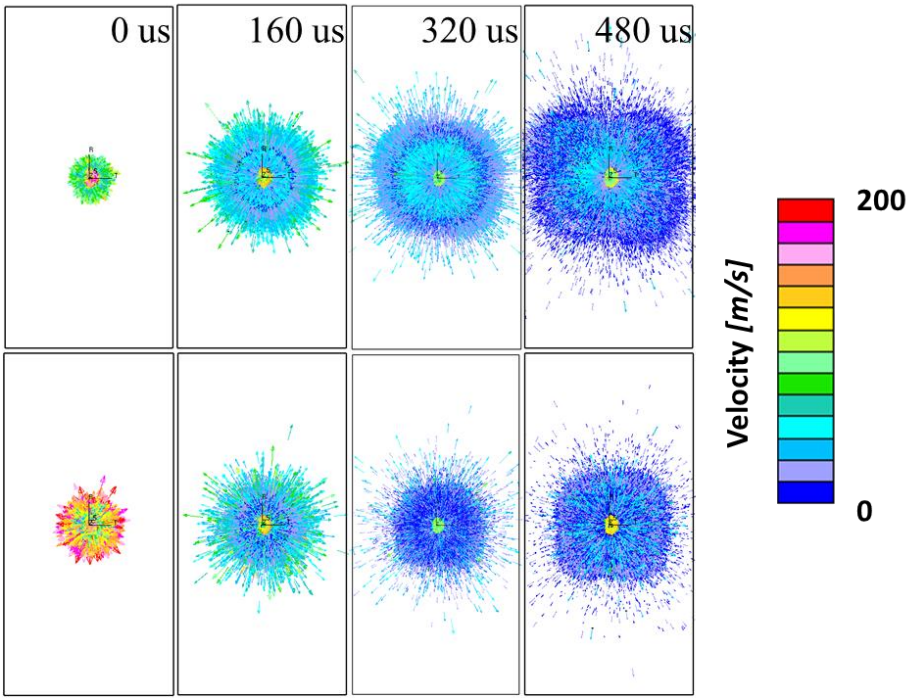

Figure 30. Top view of velocity plot by Kim model(top),
and Bai model (bottom)

The radial momentum transfer is well captured on figure 29. The number of child droplet derived from parent droplet is increased from two to four to consider 2-D spray-wall impingement phenomenon in Kim model. By increasing the number of the child droplets, it is possible to consider the normal and tangential momentum component. However, only two child droplets are generated from parent droplet. Thus, it has limitation that radial momentum transfer is considered solely in bai model. While the results of the bai model in the above figure shows symmetric shapes, the local differences were shown well in the Kim model.

5.2 Wall Film model

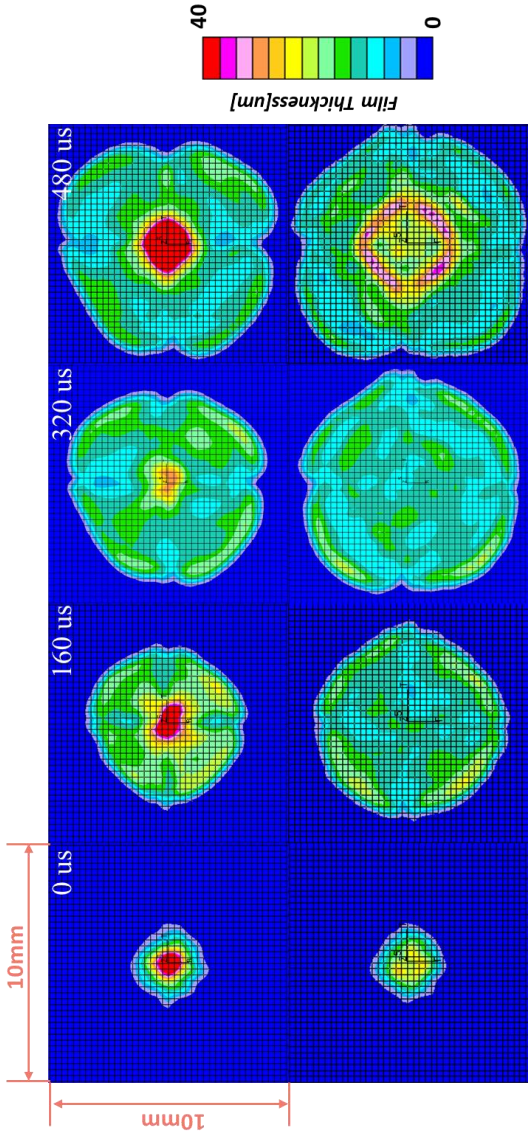

Figure 31. Top view of film shape by Kim model(top),

and Bai model (bottom)

As described in figure 30, the film of Kim model is less spread than bai model because child droplets have greater kinetic energy. The 2-D momentum transfer allows the local pressure, angular momentum difference to make partial difference. However, only radial momentum is main source of film movement in Bai model. Thus, the film seems like symmetric. Moreover, film is spread further due to the droplet tangential momentum is suppressed by model constant. As time goes by the momentum of spray plume is reduced, thus the center of the film increases its thickness in Kim model. In contrast, the film spread well because of the relatively high film momentum which is determined by model constant in bai model.

Chapter 6. Conclusions

In this thesis, a spray-wall impingement model including proper energy dissipation was developed. The splash regime of the model is modified to consider 2-D momentum transfer by increasing the number of child droplets derived from parent droplet. Considering modified spray-wall impingement model, the interacting film model was also developed.

The previous models showed less consideration in 4 parts. First, the energy dissipation amount in specific condition is too small to reduce kinetic energy of parent droplet. Moreover, the tangential velocity of child droplet is determined by model constant regardless energy equation. Second, the model assumed that diameter of child droplet is evenly distributed under parent droplet diameter. However, the child droplets follow the Rosin-Rammler distribution. Third, the splash phenomenon is simulated on horizontal plane. Thus, previous model allows only radial momentum transfer. At last, the momentum source of film is not fully considered. However, four problems mentioned above were corrected thanks to energy dissipation equation, increased number of child droplets, and modified film momentum continuity equation.

The modified spray-wall impingement model allows proper energy dissipation in DISI engine condition which the speed of parent droplet is faster than diesel engine due to longer penetration length. The energy dissipation amount is calculated in specific range of parent droplet kinetic energy. Also, the child droplet velocity is fully calculated by energy equation. It allows the model can offer rigid solution. The results of the Mundo experiments are adopted to

determine diameter of child droplet. The data shows that dimeter of child droplet has Rosin-Rammler distribution. The distribution is captured by using PDF. Thus, the diameter and velocity distribution of child droplet are more realistic behavior. The number of child droplet derived from parent droplet is increased to simulate 2-D momentum transfer. The non-symmetric droplet distribution and local film thickness are successfully described thanks to expending the droplet moving dimension from horizontal plane to 3-D domain. The modified model considers shear force, impingement momentum and local pressure difference to describe film movement. Thus, the model covers broader area ranging from the shear force dominant case such as PFI to droplet induced momentum and pressure dominant case such as DISI.

The experiment was conducted by Istituto Motori in Italy. The single hole DISI injector is used. The injector was characterized by AVL fuel injection rate meter. The temperature of the injector is controlled by J-type thermocouple and cooling cup. The plate rough ness and temperature is precisely handled. The injecting signal and TTL signal are synchronized to capture the spray behavior. Capturing both Schlieren and Mid scattering simultaneously, the optical path of both equipment uses the same way. The spray-wall impingement parameters are defined to validate model because the spray-wall impingement is complex phenomenon.

The simulation models were validated by spray-wall impingement parameter such as rebound spray radius and height. The Mie-scattering images of iso-octane spray near wall were acquired at room temperature and 150 bar injection pressure to measure rebound spray radius and height. Compared to the

existing models, the Kim model shows the best agreement with the experimental results without case-dependent changes to the model constant. The rebound spray radius and height, diameter and velocity distribution, local film thickness, and non-symmetric droplet and film distribution are improved and showed comparatively similar to the results of the experiment than Bai model.

References

1. *The International Council on Clean Transportation. Global passenger vehicle standards*. 2016 [cited 2017 May 25th].
2. Choi, K., et al., *Size-resolved engine exhaust aerosol characteristics in a metal foam particulate filter for GDI light-duty vehicle.* Journal of Aerosol science, 2013. **57**: p. 1-13.
3. Bai, C. and A. Gosman, *Development of methodology for spray impingement simulation*. 1995, SAE Technical Paper.
4. 김만식, *캐비테이션과 분무 충돌을 고려한 디젤 분무 모델 개발 = Development of diesel spray model in consideration of cavitation and spray impingement / 김만식*. 2003, 서울 : 서울대학교 대학원: 서울.
5. 조훈, *가솔린 엔진에서의 연료액막 거동 분석 = Investigation of liquid fuel film behavior in spark ignition engines / 조훈*. 2002, 서울 : 서울대학교 대학원: 서울.
6. Köpple, F., et al., *Investigation of the Parameters Influencing the Spray-Wall Interaction in a GDI Engine-Prerequisite for the Prediction of Particulate Emissions by Numerical Simulation.* SAE International Journal of Engines, 2013. **6**(2013-01-1089): p. 911-925.
7. Meredith, K., et al., *A numerical model for partially-wetted flow of thin liquid films.* Computational Methods in Multiphase Flow VI, 2011. **70**: p. 239.
8. Bai, C., H. Rusche, and A. Gosman, *Modeling of gasoline spray impingement.* Atomization and Sprays, 2002. **12**(1-3).
9. Kim, M. and K. Min, *Calculation of fuel spray impingement and fuel film formation in an HSDI diesel engine.* Journal of Mechanical Science and Technology, 2002. **16**(3): p. 376-385.
10. Mundo, C., M. Sommerfeld, and C. Tropea. *Experimental studies*

of the deposition and splashing of small liquid droplets impinging on a flat surface. in *Proceedings of ICLASS*. 1994.

11. Liu, J., et al., *Splashing phenomena during liquid droplet impact.* Atomization and Sprays, 2010. **20**(4).
12. Matsumoto, S. and S. Saito, *On the mechanism of suspension of particles in horizontal pneumatic conveying: Monte Carlo simulation based on the irregular bouncing model.* Journal of Chemical Engineering of Japan, 1970. **3**(1): p. 83-92.
13. Grant, G. and W. Tabakoff, *Erosion Prediction in Turbomachinery Resulting from Environmental Solid Particles.* Journal of Aircraft, 1975. **12**(5): p. 471-478.
14. *STAR-METHODOLOGY*. 2014.
15. Stow, C. and M. Hadfield. *An experimental investigation of fluid flow resulting from the impact of a water drop with an unyielding dry surface*. in *Proceedings of the Royal Society of London A: Mathematical, Physical and Engineering Sciences*. 1981. The Royal Society.
16. Levin, Z. and P.V. Hobbs, *Splashing of water drops on solid and wetted surfaces: hydrodynamics and charge separation.* Philosophical Transactions of the Royal Society of London A: Mathematical, Physical and Engineering Sciences, 1971. **269**(1200): p. 555-585.
17. Mutchler, C.K., *Size, travel and composition of droplets formed by waterdrop splash on thin water layers.* 1970.
18. Bai, C. and A. Gosman, *Mathematical modelling of wall films formed by impinging sprays*. 1996, SAE Technical Paper.
19. Ghadiri-Khorzooghi, H., *Raindrop Impact, Soil Splash, and Cratering*. 1978, University of Reading.
20. Meredith, K., Y. Xin, and J. de Vries, *A Numerical Model for Simulation of Thin-Film Water Transport over Solid Fuel*

Surfaces. Fire Safety Science, 2011. **10**: p. 415-428.

21. Trela, M., *A semi-theoretical model of stability of vertical falling liquid films.* Chemical engineering science, 1994. **49**(7): p. 1007-1013.
22. Fulford, G.D., *The flow of liquids in thin films.* Advances in Chemical Engineering, 1964. **5**: p. 151-236.
23. Joo, S., S. Davis, and S. Bankoff, *Two-and three-dimensional instabilities and rupture of thin liquid films falling on heated inclined plate.* Nuclear engineering and design, 1993. **141**(1-2): p. 225-236.
24. Hartley, D. and W. Murgatroyd, *Criteria for the break-up of thin liquid layers flowing isothermally over solid surfaces.* International Journal of Heat and Mass Transfer, 1964. **7**(9): p. 1003-1015.
25. Montanaro, A., et al., *EXPERIMENTAL AND NUMERICAL ANALYSIS OF A SPRAY IMPINGING ON A FLAT WALL: LIQUID/VAPOR PHASE DETECTION.* FISITA. F2016-ESYH-015, 2016.
26. Malaguti, S., et al., *Modelling of primary breakup process of a gasoline direct engine multi-hole spray.* Atomization and Sprays, 2013. **23**(10).
27. Bosch, W., *The Fuel Rate Indicator: A New Measuring Instrument for Display of the Characteristics of Individual Injection," SAE Technical Paper, SAE 660749.* 1966.
28. Montanaro, A., et al., *Schlieren and mie scattering imaging system to evaluate liquid and vapor contours of a gasoline spray impacting on a heated wall*. 2015, SAE Technical Paper.
29. Kiriliov, A. *AForge.NET C# framework*. 2013.
30. Zhao, L., et al., *An Experimental and Numerical Study of Diesel Spray Impingement on a Flat Plate.* SAE International Journal of

Fuels and Lubricants, 2017. **10**(2017-01-0854).

31. Yakhot, V. and S.A. Orszag, *Renormalization-group analysis of turbulence.* Physical review letters, 1986. **57**(14): p. 1722.
32. Gosman, A. and E. Loannides, *Aspects of computer simulation of liquid-fueled combustors.* Journal of Energy, 1983. **7**(6): p. 482-490.
33. O'Rourke, P.J., *Collective drop effects on vaporizing liquid sprays*. 1981, Los Alamos National Lab., NM (USA).
34. Nordin, P., *Complex chemistry modeling of diesel spray combustion*. 2001: Chalmers University of Technology.

실린더내 직분사 엔진에서의 벽면 충돌 및 액막 모델링

서울대학교 기계항공공학부
기계공학과
김정현

요 약

CO2 배출량이 자동차의 연비와 직접적인 관계가 있기 때문에, 일반적인 엔진보다 연비가 좋은 실린더 내 직 분사 엔진에 대한 관심이 최근 증가하고 있다. 냉각효과와 높은 체적효율 그리고 높은 압축비는 주된 실린더 내 직 분사 엔진의 장점이다. 하지만 냉시동시 분무된 액적이 벽면에 부착되어 액막을 만들고, 충분히 증발되지 않아 부분적으로 농후한 혼합기를 만드는 현상은 입자상 물질을 만드는데 최근 이에 관련된 관심이 증가하고 있다. 많은 수의 엔진 형상과 분사 전략을 실험을 통해 연구하는 방법은 비용과 시간이 많이 든다. 따라서 신뢰성이 확보된 시뮬레이션 모델이 개발되면, 이러한 엔진 개발 비용을 줄여 줄 수 있다.

정확한 입자상 물질 배출량을 예측하기 위하여, 벽면 충돌 후의 스프레이와 액막의 거동이 정확하게 예측 되어야 한다. 따라서 정확한 스프레이 모델과 액막 모델은 입자상 물질 모델에 선행되어야 한다. 과거에 만들어진 모델들은 상대적으로 큰 오류를 실험과 비교했을 때 보여준다. 분무 충돌 높이는 실험 값과 비교했을 때 과도하게 예측되고 액막의 넓이는 적게 예측된다. 이러한 시뮬레이션과 실험사이의 오류의 발생 원인은 잘못된 가정으로부터 기인한다. 과거의 모델들은 디젤 엔진에서의 고압 분무처럼 분무 관통길이가

짧아서 낮은 속도에서의 충돌만 고려하여 모델이 만들어졌다. 따라서 소멸되는 에너지가 웨버 수와 표면장력 에너지를 고려해 주는 것으로 계산될 수 있었다. 하지만 현재 실린더 내 직분사 엔진처럼 고속의 충돌에서는 액적의 운동에너지가 크기 때문에 이 두가지만으로 의미 있는 에너지 소멸이 일어나지 않는다. 따라서 이번에 수정한 모델에서는 소멸에너지를 액적의 운동에너지를 고려하여 특정 범위 안에서 결정하였다. 그 결과로 모델 상수를 줄이는 효과도 가져올 수 있었다. 2차원 벽면 충돌 현상을 고려하려고 쪼개지는 액적을 2개에서 4개로 증가시켰다. 이렇게 증가된 액적은 성공적으로 수평, 수직방향 운동량 변화를 모사하였다.

수정된 모델은 iso-octane을 사용한 미 산란 그리고 슐리렌 실험과 비교하였다. 충돌 반지름과 충돌 높이가 측정 되었고 실험과 비교 되었다. 이전의 모델과 비교해 보았을 때, 수정된 모델은 모델 상수를 변경하지 않았음에도 가장 좋은 정확도를 보였다.

주요어: 벽면 충돌 모델, 벽면 액막, 전산 유체 역학, 미 산란, 실린더 내 직분사 엔진

학 번: 2012-22712